Computer-Aided Civil and Infrastructure Engineering **18** (2003) 113–120

A Multi-Frequency Electromagnetic Image System

Qing Zhang, Xuemin Chen, Xiuhan Jiang & Ce Liu*

Department of Electrical and Computer Engineering, University of Houston, Houston, Texas 77204-4005

Abstract: *A digital, multi-frequency electromagnetic image system is developed based on the induction principle for subsurface imaging near a sewage pipe. This system, which features a broadband operation, can transmit sinusoidal in a frequency range of 1.25 KHz to 10 KHz. A microprocessor is used for all controls and computations for both the transmitter and receiver circuits. Synchronous sampling is used for digitization in order to compute the phase as well as the amplitude of the receiving signal. The system operates in the frequency domain and both the phase and amplitude information can be computed through a digital signal-processing algorithm. Test results indicate that the multi-frequency EM sensor is superior in both the missing manhole detection and general subsurface conductivity imaging to the conventional single-frequency sensors. For loop antennas with a spacing of 0.5 m, the system has a phase resolution of about 1° and an amplitude resolution of about 0.5%.*

1 INTRODUCTION

Three electromagnetic (EM) methods, widely used for shallow subsurface mapping, are ground-penetrating radar, time-domain EM, and frequency domain conductivity. Each method has limitations, either site specific or inherent in the instrument design (Stewart et al., 1994).

Ground-penetrating radar (GPR) is very useful for sounding and profiling in resistive environments. This method has excellent vertical and lateral resolution and a depth range from a few centimeters to tens of meters (Davis and Annan, 1989; Beres and Haeni, 1991). However, the depth range for a GPR is limited in materials with resistivity less than 30 Ω m (Olhoeft, 1986).

Transient EM soundings are limited by a minimum depth of investigation, above which only the integrated conductance of the overlaying section can be resolved. Thus, even under the best conditions, existing transient EM instruments cannot be used for the detailed investigation of the first 5 m of the earth (Spies, 1989; Hoekstra and Blohm, 1990).

The terrain conductivity instruments operate at low frequencies and have relatively short coil spacing. They are very effective for mapping lateral variations in conductivity. However, as sounding tools, they are good for only rudimentary interpretation of vertical conductivity variation (Moran and Kunz, 1962; Anderson and Gianzero, 1982; Shen, 1991). The key part of a terrain conductivity instrument is the sonde consisting of coil-type antennas. One or more transmitting antennas and receiving antennas may be used in an induction-sensing tool. The currents in transmitting antennas generate primary magnetic fields. By induction, eddy currents are created in the surrounding conductive medium. These currents will induce secondary magnetic fields that are received by the receiving coil. Variations of the conductivity of the surrounding medium will result in the phase and amplitude changes in the received signal (Barber, 1985). By detecting these variations, useful information can be obtained. In designing a sensor for sewage pipe imaging, soil properties surrounding the pipe is a determining factor (Huang, 1993).

In cooperation with the City of Houston, the Subsurface Sensing Laboratory at the University of Houston has successfully developed a manhole detector system, which offers higher resolution and lower cost in detecting missing manholes by using the terrain conductivity method (He, 1997). However, it operates with only a fixed frequency, which limits its applications in more advanced subsurface investigations.

The advantages of the multi-frequency induction sensing are obvious. The idea of using multiple frequencies stems from the so-called "skin-depth," also known as the depth exploration, which is inversely proportional to frequency: a low-frequency signal travels far through a conductive earth and "sees" deep structures;

*To whom correspondence should be addressed. E-mail: *cliu@uh.edu.*

© 2003 *Computer-Aided Civil and Infrastructure Engineering*. Published by Blackwell Publishing, 350 Main Street, Malden, MA 02148, USA, and 108 Cowley Road, Oxford OX4 1JF, UK.

a high-frequency signal can travel only a short distance and "see" only shallow structures. Therefore, scanning through a frequency window is equivalent to depth sounding. Depth sounding by changing the transmitter frequency is called "frequency sounding," which measures the target response at many frequencies in order to image the subsurface structure. Because the method involves a fixed transmitter-receiver geometry, it produces extremely precise, sensitive, and thermally stable measurements. In contrast, depth sounding by changing the separation between the transmitter and receiver is called "geometrical sounding," which usually requires multiple operators tending separate coils connected by wires and measuring consoles. Maintaining a precise coil separation is very difficult to the extent that some measurements (e.g., in-phase components) are often abandoned. For a shallow survey, the frequency sounding method offers high spatial resolution, high survey speed, low logistic, and high data accuracy (Won et al., 1996).

2 INDUCTION SENSING PRINCIPLE

Figure 1 shows the structure of the antenna of the multifrequency EM sensor. The antenna contains a transmitter coil and receiver coil separated by about 2.5 ft. Such geometry is called bistatic configuration. It also contains a third "bucking coil," which removes the primary field from the receiver coil.

The receiver measures the in-phase and the quadrature components of the total (primary plus secondary) magnetic fields, where the primary field is the direct coupling between the transmitting coil and the receiving coil, and the secondary field is caused by the induced currents in the media.

For the bistatic configuration, the direct coupling between the transmitting coil and the receiving coil generates an electromotive force in the receiving coil, which is given by

$$Vx = -i\omega M_{TR} I = -\frac{i\omega\mu n_T n_R S_0^2}{2\pi L^3} I \qquad (1)$$

where

- M_{TR}: mutual inductance
- n_R: number of turns in the receiving coil
- n_T: number of turns in the transmitting coil
- S_0: area of the transmitting coil
- I: current in the coil, and $I = I_0 e^{j\omega t}$
- ω: transmitting frequency

The eddy currents, which flow in circular paths coaxial with the sonde in the surrounding medium, create a secondary magnetic field. The receiving coil responds to it with an electromotive force proportional to eddy currents and thus to the conductivity of the medium (Weber, 1950). The secondary electromotive force in the receiving coil generated by the eddy currents is given by

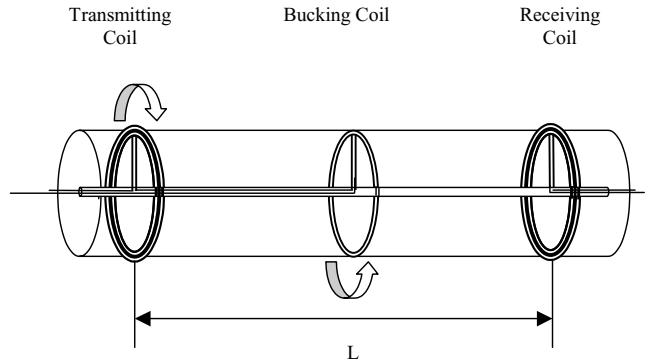

Fig. 1. Structure of the antenna.

$$V_R = -\frac{\omega^2\mu^2 n_T n_R S_0^2 I}{4\pi L}\sigma_a \qquad (2)$$

where σ_a is defined as apparent conductivity and is a function of the geometry factor. Detailed discussion on the geometry factor is given in references (Duesterhoeft, 1961; Duesterhoeft and Smith, 1962). The direct-coupled signal V_x does not contain any useful information but presents a large background noise in the received signal. For the bistatic configuration, the direct coupling signal detected by the receiving coil can be two orders of magnitude greater than the induced signal. While removing the sonde error completely is difficult to achieve in practice, it is possible to nullify most of the direct signal by a third bucking coil in the middle of the transmitter and receiver. In order to cancel the background signal, the bucking transmitting coil should be anti-wounded with the main one; the number of turns and the distances between the bucking coil and the receiving coil should satisfy

$$\frac{n_1}{n_2} = \frac{L^3}{(L/2)^3} = 8 \qquad (3)$$

where n_1 and n_2 are the number of turns of transmitting coil and bucking coil respectively.

At present, it is impractical to measure the normalized components because it requires exact knowledge of the primary field phase and amplitude as well as long-term stability of the instrument gain and phase shift (Stewart et al., 1990). Accurate measurement of the primary field would require suspending the instrument high in the air to reduce reflected energy from the earth's surface. Additionally, the instrument gain and phase shift are sensitive to temperature and metallic cable geometry. The measured primary field is useless without monitoring the

instrument temperature, the placement of certain cables, and the precise temperature dependence of the instrument response (Huang, 1993).

Electrical solutions to the above problems are possible but are not reliable for routine instrument use. A practical solution is to measure the amplitude and phase difference of the signal in the receiving coil. The unknown primary normalization factor is removed by the amplitude ratio, and the unknown primary phase reference is removed by the phase difference. Secondly, during the time the instrument measures and records all field components for each frequency, the instrument temperature and geometry are effectively constant; thus, the unknown geometry effect and temperature-dependent gain and phase shift are also constant and are removed by the calculation.

3 SIGNAL PROCESSING

The fact that V_X is 90° out of phase with V_R enables the use of a phase detector in the receiving circuits to obtain useful information.

In the manhole detector system, an analog switch followed by a low-pass filter is used to detect the phase change. The circuitry implemented in the manhole detector is neat and works very well with a single frequency. However, in this analog approach, all the filtering works only with fixed frequency; therefore, it is not suitable to operate in multi-frequency situations. Furthermore, in the manhole detector, the receiver has to send the signal to the ground by analog transmission techniques. The noise can be easily picked up during transmission, which severely affects the accuracy of the measurement.

In the multi-frequency EM sensor, the signal picked up at the receiver is digitized at a rate of 40 kHz and with a 16-bit resolution A/D converter. In order to extract the in-phase and quadrature components, a discrete Fourier transform (DFT) to the sampling sequence is then carried out. This DFT operation renders an extremely narrow-band, matched-filter-type, signal-equals-detection technique (Lathi, 1998). The basic steps in applying the DFT to a continuous-time signal are indicated in Figure 2. The anti-aliasing filter is incorporated to eliminate or minimize the effect of aliasing when the continuous-time signal is converted to a sequence. The need for multiplication of x[n] by w[n] (i.e., windowing) is a consequence of the finite-length requirement of the DFT.

In the multi-frequency EM system, a continuous-time sinusoidal signal is measured, which can be expressed as

$$s(t) = A_0 \cos(\Omega_0 t + \theta_0) \qquad 0 < \mathrm{t} < \infty \tag{4}$$

Assuming ideal sampling with no aliasing and no quantization error, the discrete-time signal can be obtained by

$$x[n] = A_0 \cos(\omega_0 n + \theta_0), \qquad 0 < n < \infty \tag{5}$$

where $\omega_0 = \Omega_0\, T$. The windowed sequence of x[n] is then

$$v[n] = A_0 w[n] \cos(\omega_0 n + \theta_0) \tag{6}$$

Its Fourier transform can be expressed as

$$V(e^{j\omega}) = \frac{A_0}{2} e^{j\theta_0} W\left(e^{j(\omega-\omega_0)}\right) + \frac{A_0}{2} e^{-j\theta_0} W\left(e^{j(\omega+\omega_0)}\right) \tag{7}$$

the rectangular window, which has Fourier transform of

$$W(e^{j\omega}) = \sum_{n=0}^{L-1} e^{-j\omega n} = e^{-j\omega(L-1)/2} \frac{\sin(\omega L/2)}{\sin(\omega/2)} \tag{8}$$

According to Equation (7), the Fourier transform of the windowed signal consists of the Fourier transform of the window replicated at frequencies $\pm\omega_0$ and scaled by the complex amplitudes of the individual complex exponential that make up the signal.

Consider the system of Figure 2 and in particular $W(e^{j\omega})$ and $V(e^{j\omega})$ for the specific case of sampling rate $1/T = 40$ kHz and a rectangular window w[n] of length 32. Suppose a sinusoidal signal is $\Omega_0 = 2\pi \times 10^4$ (10 kHz) or, equivalently, $\omega_0 = 2\pi/4$. Then the windowed sequence of this sinusoidal signal is

$$v[n] = \begin{cases} A_0 \cos\left(\frac{2\pi}{4} n\right), & 0 \le n \le 31, \\ 0, & \text{otherwise} \end{cases} \tag{9}$$

Figure 3a shows the windowed sequence of this sinusoidal signal. The magnitude of the 32-point DFT of v[n] is shown in Figure 3c and corresponds to the samples of $|V(e^{j\omega})|$, which is plotted in Figure 3b. From Figure 3c,

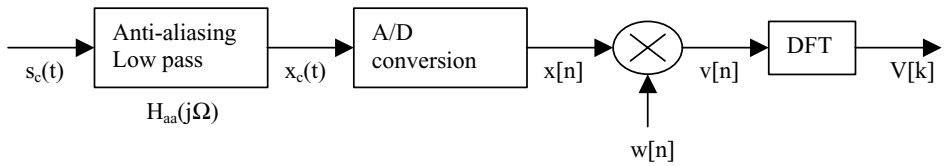

Fig. 2. Processing steps in the DFT analysis of a continuous time signal.

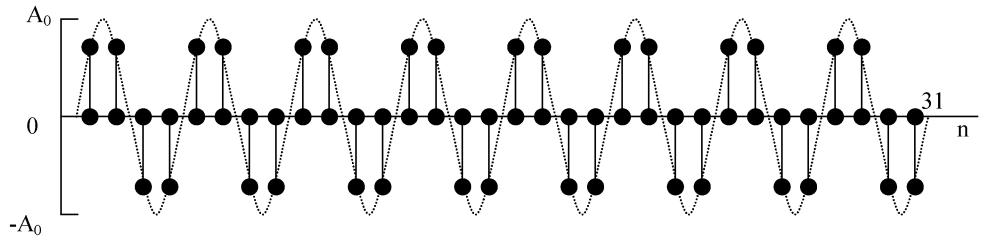

(a) Windowed signal

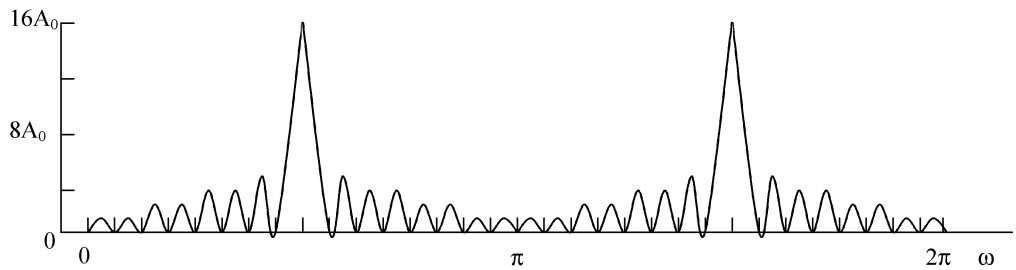

(b) Magnitude of discrete-time Fourier transform ($|V(e^{j\omega})|$)

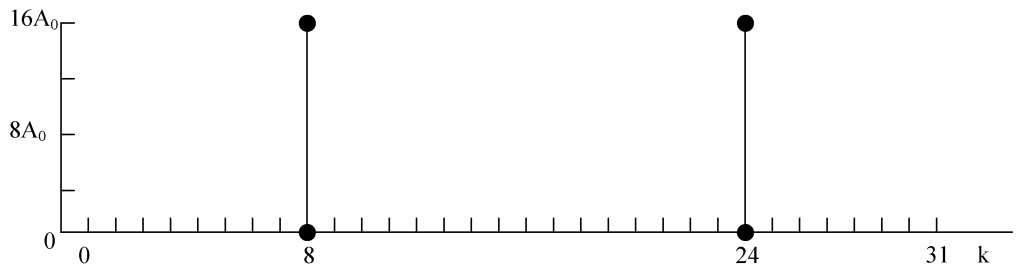

(c) Magnitude of DFT

Fig. 3. Discrete Fourier analysis of windowed sinusoidal signal.

one can see that the Fourier transform is exactly zero at frequencies that are sampled by the DFT except those points at k = 8 and 24.

As mentioned previously, the DFT of the windowed sequence v[n] provides samples of $V(e^{j\omega})$ at the N equally spaced discrete-time frequencies $\omega_k = 2\pi k/N$, k = 0, 1, ..., N − 1. Specifically, for the windowed sequence with N = L = 32, the frequency $\omega_0 = 2\pi k/32 = 2\pi/4$ corresponds exactly to the DFT sample k = 8. Equation (10) is used to calculate the phase and amplitude information of the original sinusoidal signal.

$$V[8] = \sum_{n=0}^{31} v[n]e^{-j(2\pi/32)8n} = \frac{A_0}{2}e^{j\theta_0}W(0) = 16A_0e^{j\theta_0} \tag{10}$$

4 SYSTEM IMPLEMENTATION

Figure 4 shows the block diagram of the multi-frequency EM sensor. From Figure 4, one can see that a coil-typed antenna, a transmitter, and a receiver form the core of the multi-frequency EM sensor. A microcontroller with data acquisition (DA) board at the receiver takes care of all the control logic of the system.

During the operation, four frequencies are transmitted sequentially in binary steps over the range 1.25 kHz to 10 kHz. The transmitting signal is derived from a reference square wave signal generated by the microcontroller at the receiver end. The reference square wave signal is divided by four by a couple of flip-flops and fed to a programmable band-pass filter. After the band-pass filtering, a single frequency sinusoidal signal is obtained.

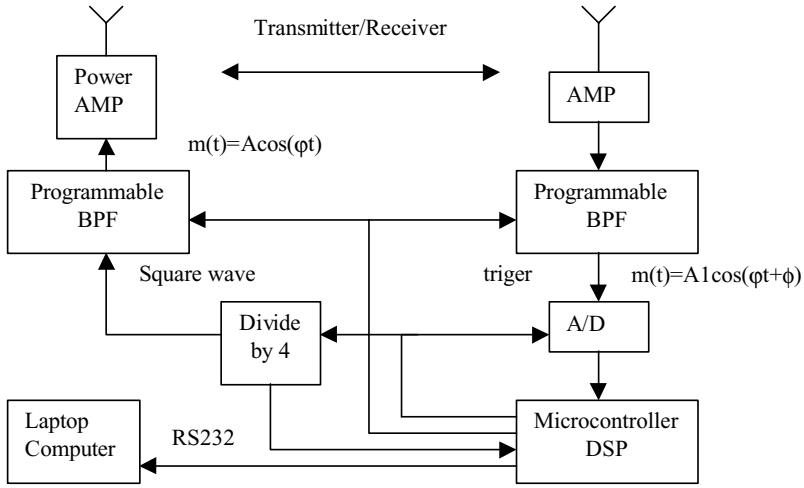

Fig. 4. Block diagram of the multi-frequency EM sensor.

The sinusoidal signal is amplified by a power amplifier and sent to the transmitting coil. The microcontroller controls the tuning of the programmable band-pass filter via digital I/Os.

The signals received at the receiver are amplified, sent to the programmable filter, and then digitized by the data acquisition board. The A/D conversion is triggered by the square wave from which the transmitting sinusoidal is derived. This synchronous sampling technique helps detect the phase as well as the amplitude change of the transmitting signal. The microcontroller processes the digitized data in order to get the amplitude and phase information and sends the information to a laptop via RS232 for further processing.

In the field test, since the signal needs to be transmitted over 500 ft, RS485 protocol is used to transmit the digital phase and amplitude signal to the host computer above the ground. A couple of RS232 to RS485 converters are used for the protocol conversion.

The transmitting circuits, the antenna and the receiving circuits are mounted in a section of 4-inch-diameter PVC pipe. The transmitting circuits and the receiving circuits are shielded with two aluminium boxes and are placed on opposite sides of the antennae. Since the relative position of these boxes has significant influence on induction, all the components and wires are tightly mounted in the PVC pipe to prevent them from shifting during the testing. The photograph of the all-system assembly is shown in Figure 5.

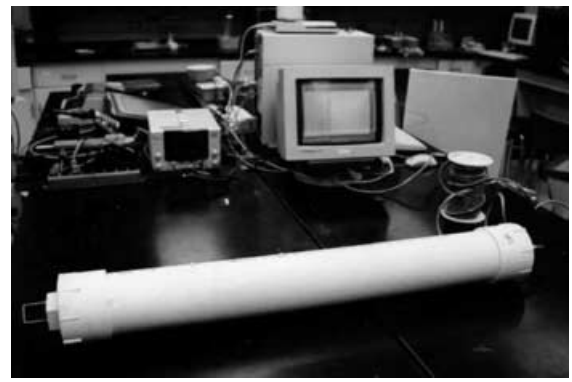

Fig. 5. The structure of the multi-frequency EM sensor.

5 SYSTEM PERFORMANCE

5.1 Sensitivity of the system

Tests of the system sensitivity were made by hanging the system high in the air and by varying the loop space from 10 cm to 1 m. For short spacing, the instrument can resolve changes on the order of 2.1° phase and 0.5% amplitude. Resolution at longer spacing is degraded due to the low signal strength. In the lab environment, the resolution for spacing of up to 4 m is tested and is at about 5° phase and 5% amplitude. The phase and amplitude resolutions versus loop spacing are shown in Figure 5a and b.

The loop spacing has an optimum point where the sensitivity of the system is highest. Longer loop spacing will result in greater investigation depth. However, due to reduced signal-to-noise ratio, big loop spacing will reduce the received signal strength and therefore reduce the system resolution. The loop spacing in the prototype device is chosen to be 0.5 m for best system performance. With this configuration, phase resolution is about 1° and amplitude resolution is about 0.5%.

5.2 Lab test

The EM sensor is very sensitive to ferrous material. The EM sensor is tested with a 3 × 5 × 10 inch metal box.

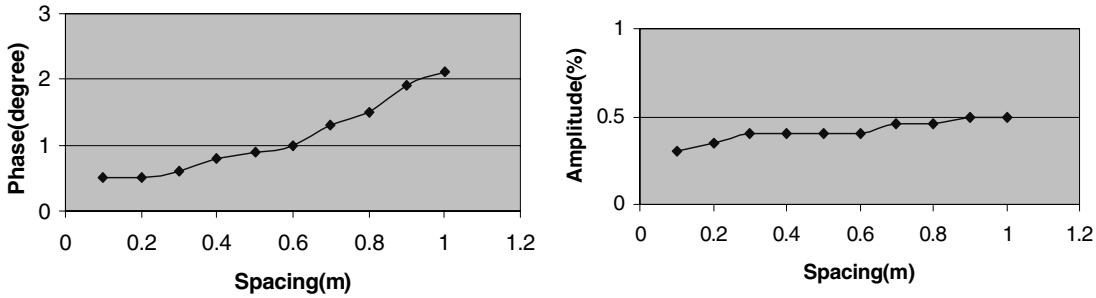

(a) Phase resolution (b) Amplitude resolution

Fig. 6. Phase and amplitude measurement vs. loop space.

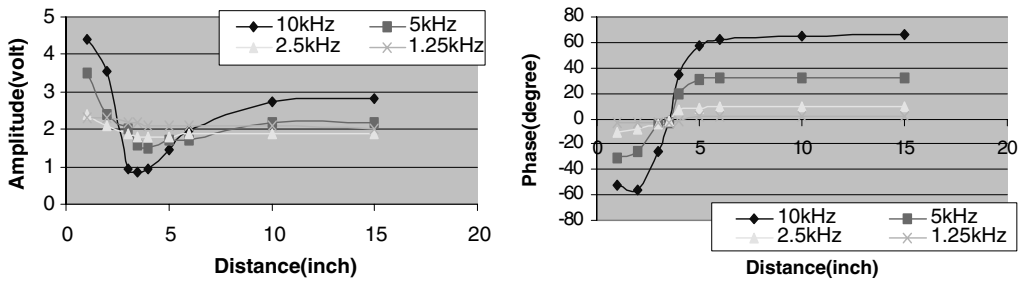

(a) Amplitude response (b) Phase response

Fig. 7. Phase and amplitude measurement vs. distance change.

Figure 7 shows how the phase and amplitude respond when the metal box vertically approaches the antenna. At 10 kHz, the change in phase and amplitude is significant when the metal box is within 6 inches of the antenna. However, when the transmitting frequency decreases, the change in phase and amplitude is not significant. At 1.25 kHz, the existence of the box is not detectable.

As we discussed earlier, the directed electromotive force V_R is proportional to the transmitting frequency ω, while the secondary electromotive force V_X generated by the eddy current is proportional to ω^2. Therefore when ω decreases, both the in-phase and the quadrature components in the receiver will be reduced. As a result, the amplitude of the signal picked up by the receiver will decrease. Also notice that V_X/V_R is proportional to ω, so when ω decreases, the phase change is also going to decrease. When ω is too small, the signal and the noise at the receiver will be on the same level, which makes the metal box not detectable at 1.25 kHz. In conclusion, the transmitting power needs to be increased at lower frequency in order to maintain the same signal-to-noise ratio at the receiver.

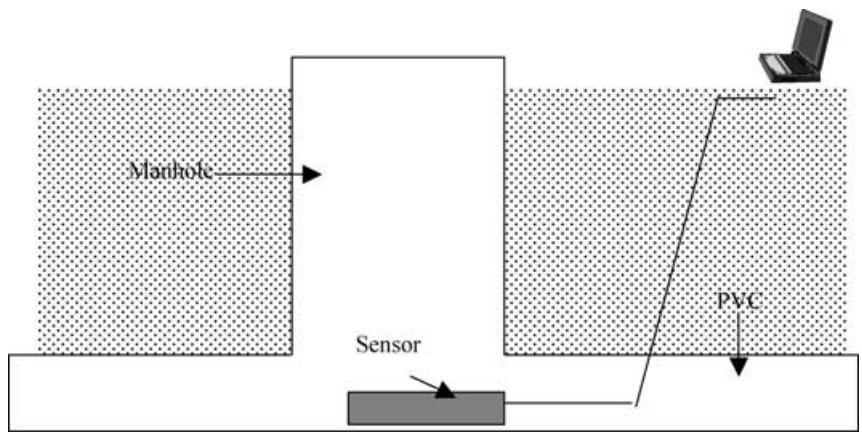

Fig. 8. Testing set-up for manhole detection.

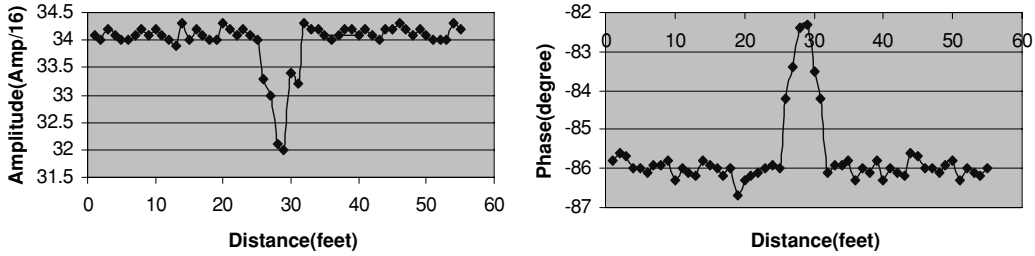

(a) Amplitude response in different media (b) Phase response in different media

Fig. 9. Manhole test result.

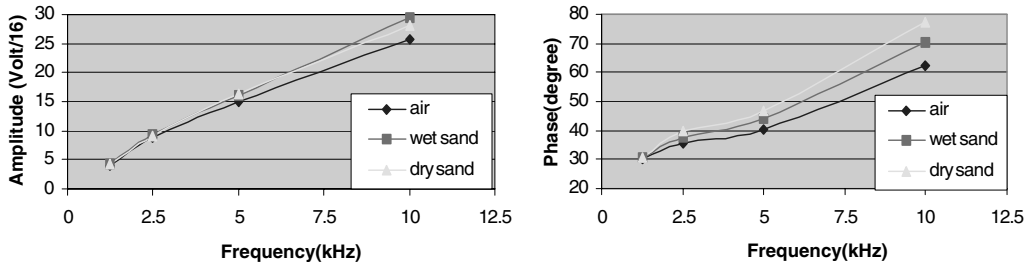

Fig. 10. Effect of different media.

5.3 Field test

The lab test shows that the system developed is very sensitive to metal. Since the system will finally be used by the City of Houston to detect missing manholes and inspect sewage pipe, field tests have been carried out to ensure that the system works with the changes of conductivity.

The conductivity of soil near a sewage pipe and manhole along the sewer pipes varies from 0.01 S/m to 0.1 S/m in most cases. However, the conductivity drops to less than 0.005 S/m inside a manhole filled with air. Results of numerical simulation have proven that this kind of change in conductivity is detectable using a properly designed tool (Huang, 1993).

To save labor, an underground sewer pipe was built with a manhole in the middle at the main campus of the University of Houston. The sewer pipe is 8 inches of concrete pipe with a total length of 55 ft. The structure of the test set-up is shown in Figure 8.

The result of the field test is shown in Figure 9. The test begins as the sensor head, starts to move into the sewer pipe from the right-hand side, and stops when the sensor comes out at the left-hand side. For maximum sensitivity, the operating is fixed at a frequency of 10 kHz. Figure 9 demonstrates that when the sensor is in the manhole, both the phase and amplitude of the signal at the receiver change. The phase changes about 4° and the amplitude changes about 6%, which is detectable with the system resolution. The overall performance of the system is satisfactory according to the results of the field tests.

Figure 10 shows the phase and amplitude response when the sensor is placed in a sewage pipe surrounded by different media.

One can see that the phase has obvious changes when the sensor is in different media. However, amplitude change is not as obvious as that of the phase, especially when the signal is below 5 kHz. The reason is that the received signal is the superposition of direct coupling signal and induced signal. The direct coupling signal is still stronger than the induced signal even using the bucking transmitting coil. The amplitude of the direct coupling signal will not change with the surrounding material, and the induced signal at the receiver becomes weaker at the low frequency as we discussed in Section 5.2.

Finally, the detectability of the EM sensor is tested using the method shown in Figure 11. The sensor is buried under the wet sand with a cylindrical hole filled with air. For maximum detectability, the frequency is fixed at 10 kHz. The test result is shown in Figure 12a and b.

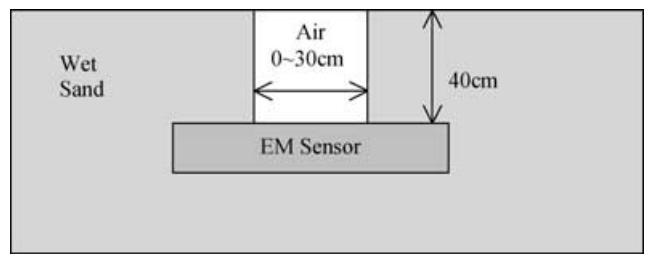

Fig. 11. Detectability test set-up.

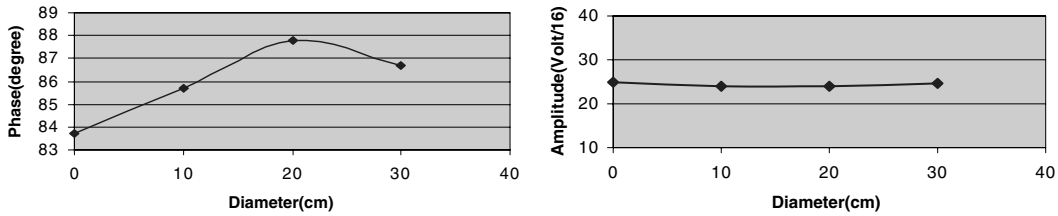

(a) Phase changes (b) Amplitude changes

Fig. 12. Detectability test result.

Figure 12a shows that the 10 cm "air cylinder" is detectable by monitoring the phase response of the EM sensor. However, as shown in Figure 12b, the amplitude change is not detectable within the system resolution.

6 DISCUSSION AND CONCLUSION

The digital, multi-frequency EM sensor provides significant advantages over the analog, single-frequency sensor for shallow environmental characterization. The new system features a broadband operation in a frequency range of 1.25 kHz to 10 kHz. Unlike the manhole detector, the phase and amplitude are computed by the digital signal processing (DSP) microcontroller in the sensor head before sending the data out. Therefore, the noises added during transmission are greatly reduced. It operates in the frequency domain and both the phase and amplitude information can be computed through DSP algorithm. With efficient software implementation, the low-cost DSP data acquisition board designed for the system is capable of sampling at 40 kHz and has 14–15 bits of resolution.

The test results demonstrate the feasibility of the new multi-frequency EM sensor in both the missing manhole detection and general terrain conductivity measurement. For a loop spacing of 0.5 m, the system has a phase resolution of about 1° and an amplitude resolution of about 0.5%.

ACKNOWLEDGMENTS

This project is sponsored by the National Science Foundation, Texas Higher Education Coordinate Board, City of Houston, and Montgomery Watson Co.

REFERENCES

Anderson, B. & Gianzero, S. (1982), Induction sonde in stratified media, *The Log Analyst*, **24**, 25–31.

Barber, T. D. (1985), Introduction to the phasor dual induction tool, *Journal of Petroleum Technology*, **37**(10), 1699–706.

Beres, M. & Haeni, F. P. (1991), Application of ground-penetrating radar method in hydrogeologic studies, *Ground Water*, **29**, 375–86.

Davis, J. L. & Annan, A. P. (1989), Ground-penetrating radar for high resolution mapping of soil and rock stratigraphy, *Geophysics*, **37**(4), 516–49.

Duesterhoeft, J. R. (1961), Propagation effects in induction logging, *Geophysics*, **26**(2), 192–204.

Duesterhoeft, J. R. & Smith, H. W. (1962), Propagation effects on radial response in induction logging, *Geophysics*, **27**(4), 463–9.

He, M. (1997), Manhole-detector system, Master's Thesis, University of Houston.

Hoekstra, P. & Blohm, M. W. (1990), Case histories of time domain electromagnetic soundings in environmental geophysics, *Society of Explore Geophysics*, **2**, 1–15.

Huang, M. (1993), Resistivity measurement in laboratory and field environments, Master's Thesis, University of Houston.

Lathi, B. P. (1998), *Modern Digital and Analog Communication Systems*, Oxford University Press, New York.

Moran, J. H. & Kunz, K. S. (1962), Basic theory of induction logging and application to study of two-coil sondes, *Geophysics*, **27**(6), 829–58.

Olhoeft, G. R. (1986), Direct detection of hydrocarbon and organic chemicals with ground penetrating radar and complex resistivity, *Ground Water*, **16**, 284–304.

Shen, L. C. (1991), Theory of a coil-type resistivity sensor for MWD application, *The Log Analyst*, **32**(5), 603–11.

Spies, B. R. (1989), Depth of investigation in electromagnetic sounding methods, *Geophysics*, **54**, 872–88.

Stewart, D. C., Anderson, W. L., Grover, T. P. & Labson, V. F. (1990), New instrument and inversion program for near-surface mapping: High-frequency EM sounding and profiling in the frequency range 300 kHz to 30 MHz, *60th Annual International Meeting: Society of Exploring Geophysics*, 410–13.

Stewart, D. C., Anderson, W. L., Grover, T. P. & Labson, V. F. (1994), Shallow subsurface mapping by electromagnetic sounding, *Geophysics*, **59**(8), 1201–10.

Weber, E. (1950), *Electromagnetic Fields Theory and Applications, Vol. I, Mapping of Fields*, John Wiley & Sons, New York.

Won, I. J., Keiswetter, A., George, R., Fields, A. & Sutton, L. C. (1996), GEM2: A new multi-frequency electromagnetic sensor, *Journal of Environmental and Engineering Geophysics*, **1**, 129–37.